JOURNAL OF THE ROYAL SOCIETY Interface

J. R. Soc. Interface (2008) **5**, 1009–1022
doi:10.1098/rsif.2007.1313
Published online 29 January 2008

Nanomechanical evaluation of nickel–titanium surface properties after alkali and electrochemical treatments

Wojciech Chrzanowski[1,4], Ensanya Ali Abou Neel[1], David Andrew Armitage[2], Kevin Lee[3], Witold Walke[4] and Jonathan Campbell Knowles[1,*]

[1]*Division of Biomaterials and Tissue Engineering, UCL Eastman Dental Institute, 256 Gray's Inn Road, London WC1X 8LD, UK*
[2]*Department of Engineering, University of Leicester, Leicester LE1 7RH, UK*
[3]*London Center for Nanotechnology, 17–19 Gordon Street, London WC1H 0AH, UK*
[4]*The Silesian University of Technology, Institute of Materials Science and Biomaterials, ul. Konarskiego 18a, Gliwice 44-100, Poland*

In this paper, the suitability of alkali treatment followed by heat treatment at 600°C, and spark oxidation for nickel–titanium, intended for medical applications such as pins, wires and clamps, was evaluated on the basis of nanomechanical and wear testing. In addition, the chemical composition and topography of the surface layer, wetting ability, corrosion resistance and influence of the heat treatment on structure of the alloy were also investigated. The results showed that the highest hardness was observed for alkali-treated samples, and this could be correlated with the structure of the sample that contained martensite and a higher phase transformation temperature. This treatment caused a very large increase of nickel in the top layer and decreased resistance in pitting corrosion. These results disqualified the treatment to be considered as useful for medical applications. On the other hand, the hardness of the oxidized samples was at the same level as that obtained for ground reference samples. Moreover, the oxide layer was enriched with phosphorus, and it was predominantly composed of TiO_2 and phosphorus oxides. This 3.1 μm thick layer had good adhesion to the substrate as indicated by scratch testing and wear resistant in nanowear testing. However, the oxidation did not significantly increase the corrosion resistance of the alloy compared with reference samples.

Keywords: Ni–Ti; scratch test; nanoindentation; wear test; spark oxidation; alkali treatment

1. INTRODUCTION

The mechanical properties such as superelasticity and shape memory effects of nickel–titanium alloys (nitinol or Ni–Ti) make these materials useful for cardiovascular, urological, tracheal and dental applications. These properties could be employed for maxillofacial, orthopaedic and dental applications to ease insertion, removal of implants or introduce forces (bending, compression or tension) on the tissue to improve the healing process. To date, only a few cases have been reported where Ni–Ti alloy was used in these areas (Zheng & Huang 2001; Chu *et al.* 2005; Parashos & Messer 2005; Grosgogeat *et al.* 2006). Owing to the high nickel concentration and relatively poor wear resistance of the native surface, the use of nitinol as an implant may be of concern. However, laboratory studies showed superior wear resistance of nitinol in comparison with stainless steel (Yan 2006; Yang *et al.* 2007). The high plastic yield stresses of the transformed martensite, which is the low-temperature phase (twinned structure), in Ni–Ti hindered the occurrence of the plastic deformation, and therefore increases the wear resistance of this material. Higher wear resistance of nitinol was also due to the combined effects of lower Young's modulus, low transformation stress, large recoverable transformation strain and high plastic yield strength of the martensite (Yan 2006; Yang *et al.* 2007).

Nevertheless, some of the dental and orthopaedics applications require materials with very good wear resistance and having high adhesion of the outer layers. Commonly, the implant surface is subjected to fretting during insertion, interaction with the bone bearing the forces, and also during micromovement of the bone which is required for proper bone healing. Therefore, it seems to be critical to improve the wear properties of the implants intended for hard tissues applications. Moreover, surface properties are of great importance not only from a mechanical but also from a biological

*Author for correspondence (j.knowles@eastman.ucl.ac.uk).

Received 27 November 2007
Accepted 3 January 2008

point of view. That is why careful selection of surface treatment is crucial for implant acceptance and durability in the body.

Numerous surface modification techniques were used to improve wear and mechanical properties of implants (Chu *et al.* 2005; Cheng & Zheng 2006*a*,*b*; Grosgogeat *et al.* 2006; Ju & Dong 2006; Mändl *et al.* 2006; Ni *et al.* 2006; Liu *et al.* 2007). In general, these techniques were divided into three groups: removal; oxidation; and coating of the implant surface (Hassel 2004). When wear properties are of great concern, both oxidation and coating of the implant surface are of greatest importance (Firstov *et al.* 2002; Sul *et al.* 2006; Kawakita *et al.* 2007); it was demonstrated that titanium nitride coatings on nitinol significantly improved hardness, wear properties and adhesion to the underlying substrate (Cheng & Zheng 2006*a*). Hardening of the surface using laser alloying also gave very positive results in terms of wear resistance (Man *et al.* 2006); the plasma alloying was also shown to have an influence on tribological and corrosion properties of nitinol (Ju & Dong 2006). In both cases, the treated nitinol surface was found to be composed mainly of TiO_2 and Ni_3Ti (Ju & Dong 2006), and the thickness of this treated surface layer was greater than those of thermally oxidized surfaces that had a similar composition. This treated surface layer was also reported to have high hardness coupled with high wear resistance, which in turn enhances the tribological properties of nitinol; however, the bond of this layer was reported as fairly good (Ju & Dong 2006; Man *et al.* 2006). Nevertheless, some of the coatings, such as diamond-like coating, which has a very positive effect on nickel release, wear properties and low implant reactivity in the body (Kobayashi *et al.* 2005), could cause severe corrosion problems when this coating is impaired or could not completely seal the underlying surface. As is well known, from an electrochemical point of view, a combination of two materials with a completely different electrochemical potential will give rise to very fast corrosion of the material (Marciniak *et al.* 2007*a*,*b*).

Among the methods that were previously used to improve mainly biological properties of titanium and its alloys (Ti6Al4V, Ti6Al7Nb), thermal, alkali and electrochemical treatments are of interest to the authors (Kokubo 1998; Firstov *et al.* 2002; Chen *et al.* 2003, 2004; Shevchenko *et al.* 2004; Chrzanowski *et al.* 2005; Gu *et al.* 2005; Cheng & Zheng 2006*b*; Chrzanowski 2006; Shukla & Balasubramaniam 2006; Armitage & Chrzanowski 2007; Kawakita *et al.* 2007; Wen *et al.* 2007). Electrochemical and chemical treatment in conjunction with heat treatment improved the bioactivity through the alteration to the topography, structure and chemical composition of the surface. For nickel–titanium alloys, thermal oxidation and high-voltage oxidation (Green *et al.* 1997; Firstov *et al.* 2002; Sul *et al.* 2006; Kawakita *et al.* 2007) were shown to have an influence on the topographical features of the surface and its chemical composition. These properties were reported to be highly dependent on parameters such as temperature or anodization conditions.

It was the intention of the authors to examine, from a tribological point of view, the suitability of three types of treatments, heat, alkali and electrochemical treatment, for preparation of nickel–titanium alloy surfaces for biomedical applications. The goal of these surface treatments was to improve wear resistance of nickel–titanium alloy for hard tissues application. It is assumed that the treatment could be used for surface preparation of wires, pins, clamps, plates and elements of the distraction fixators for bone applications.

2. MATERIAL AND METHODS

In this study, nickel–titanium alloy (nitinol or Ni–Ti; Johnson Matthey, Inc.) was used in the superelastic form. Flat square (8×8 mm) samples were ground to a mirror finish on waterproof SiC paper (P# 4000 grit, Struers), cleaned in isopropanol and then ultrapure water, soaked in HNO_3 for 10 min and finally cleaned in ultrapure water. Two types of treatment were performed for the cleaned samples.

(i) Soaking a group of cleaned samples in 10 M NaOH for 24 hours, rinsing with ultrapure water, drying in air and then heat treating at 600°C for 1 hour in air (heating rate 10°C min^{-1}, rapid cooling in air).
(ii) Spark oxidizing another group of cleaned samples in $H_2SO_4+H_3PO_4$ (plasma electrolysis) with a current density of 2 mA cm^{-2} for 1 min, and electrolyte temperature of 40±5°C. After treatment, samples were rinsed with ultrapure water, and then dried in a vacuum furnace at 40°C.

Both alkali-treated and spark oxidized samples were examined and compared with untreated ground samples as references.

2.1. Surface topography and roughness

The topography of each sample surface was examined using atomic force microscopy (AFM; PSIA XE-100) in a non-contact mode. For all the sample types, three sizes of scans were done: 10×10 μm; 25×25 μm; and 40×40 μm.

The roughness of the samples was measured using a Proscan 1000 (Scantron) laser profilometer. In the measurement, the roughness parameter (R_a) was assessed. Laser profilometry measurements were carried out on the scan 5×5 mm. Additionally, R_a was also analysed on the AFM 40×40 μm images and compared with those obtained by laser profilometry.

2.2. Surface chemical composition determination

X-ray photoelectron spectroscopy (XPS; Thermo Escalab 220iXL) measurements were performed to examine chemical composition of the sample surfaces using an Al Kα monochromated X-ray source. For all the samples, both survey and detailed spectra were recorded. Detailed spectra enable precise evaluation of the chemical composition that was done using Casa XPS software v. 2.3.1.3, and in the evaluation Shirley background type was used.

2.3. Contact angle measurements

To assess wettability of the surfaces, the contact angle (CA) measurements were carried out under static (equilibrium) mode using ultrapure water as the test liquid using a KSV CAM 200 CA system (LOT-Oriel, UK). Nitinol discs from each group were used, and droplets of approximately 5 µl of ultrapure water were placed on the disc surface using a manual syringe. The drop profile was recorded at 0.1 s intervals for 1 min, and the measurements were carried out on triplicate samples.

2.4. Nanohardness test

To evaluate nanohardness of three types of samples (NT, BNT and SP), nanoindentation tests were performed using a Hysitron triboindenter. In these tests, a standard Berkovich indenter was used. To obtain a depth profile of the hardness, reduced elastic modulus and contact depth, 16 load-controlled (combined with partial unload) indents were performed on each sample. Each loading–unloading cycle consisted of a 1 s loading, a 1 s hold time and a 1 s unloading. The minimum force used for nanoindentation tests for all samples was 168.89 µN, and the specified peak force was 9 mN.

2.5. Nanoscratch test and nanotribo test

In order to assess the scratch resistance and adhesion of the films, nanoscratch test using a CSM nanoscratch tester was performed. Owing to the difference in thickness and topography of the surface, the scratch tests for alkali and spark oxidized samples were carried out using different parameters to enable the measurement to be made. The scratch tests were carried out using sphero-conical 90° indenter, $R=5$ µm (for spark oxidized sample) and 1 µm (for alkali-treated sample); scanning load was 1 mN and final loads were 50 and 20 mN for spark oxidized and alkali-treated samples, respectively.

Measurement of the friction coefficient and wear properties of the films was performed through nanotribo test using a CSM nanotribometer. These tests were conducted using a rotative mode with a normal load of 60 mN; a static ball partner made of steel 100Cr6, and $R=1.5$ mm was used in these tests.

2.6. Transformation temperature

The transformation behaviour and the characteristic temperatures of the nitinol samples treated at 600°C were determined using a Pyris Diamond DSC (Perkin-Elmer Instruments, USA) and compared with the non-treated ground samples. The instrument was calibrated using the manufacturer's instructions, with indium and zinc as standards. Discs ($n=3$) of each sample were heated from -50 to 150°C at 10°C min^{-1}. All tests were carried out under nitrogen purge. On the basis of the measurements, start and finish temperatures of austenite→martensite transformation (during heating) and martensite→austenite transformation (during cooling) were calculated. They were labelled as follows: A_s, austenite start; A_f, austenite finish; M_s, martensite start; and M_f, martensite finish. The peak temperature of these transformations was also considered.

2.7. X-ray diffraction

X-ray diffraction (XRD) analysis was carried out to set the differences in the crystallographic structure for the alkali-treated compared with the ground samples. XRD measurements were made on a Brüker D8 Advance diffractometer in θ–θ mode with Ni filtered Cu Kα radiation and detected using a Brüker Lynx Eye detector. XRD spectra were recorded in the range 2θ 38–46° at a step size of 0.0196° and a count time of 5 s.

2.8. Corrosion resistance

The corrosion tests were carried out in Hanks' Balanced Salt Solution (Gibco) using a Voltamaster 21 electrochemical set (radiometer). The tests were carried out at 36.6 ± 1°C and pH 7.9–8.2. At the beginning of the experiment, the corrosion potential (E_{cor}) was measured for 60 min, then the polarization curves were recorded. The potential was increased from $E_{cor}=100$ mV up to the potential for which the current density was equal to 1 mA cm^{-2}. Then, the direction of polarization was reversed and the return curves were also recorded. In these tests, the following parameters were established: corrosion potential, E_{cor}; polarization resistance, R_p; transpassivation (breakdown) potential, E_B; and corrosion current density, i_{cor}.

2.9. Thickness measurements of the oxide layers

To measure the thickness of the oxide layer on the samples, a Zeiss XB1540 cross-beam microscope was used. To obtain a cross section of the layers, the samples were tilted at an angle of 54° and a section of 6×8 µm was etched using a gallium ion beam. Thicknesses of the layers were measured on the recorded cross-section images for each of the samples.

3. RESULTS

3.1. Surface topography observations and roughness measurements

The laser profilometry and AFM study showed significant differences in the roughness for all three types of samples. The surface of the ground samples was smooth—roughness of 0.14 µm. On the other hand, the alkali-treated samples had more complex topographical structure of the surface, and the surface roughness was greater than that of the ground samples as given in table 1. The spark oxidized samples, however, had a rough layer exhibiting a pitted structure, as shown in figure 1. The roughness for the spark oxidized samples was the highest (approx. 0.85 µm) compared with the other samples.

Table 1. Chemical composition (at%), wettability and roughness (measured by laser profilometry (R_a) and AFM (R_a^{AFM})) of alkali-treated and spark oxidized samples compared with the ground nitinol samples that were used as a reference.

	chemical composition								contact angle	roughness	
sample	C (at%)	Ca (at%)	N (at%)	Na (at%)	Ni (at%)	O (at%)	P (at%)	Ti (at%)	Ni/Ti	CA (°)	R_a (μm)	R_a^{AFM} (nm)
ground	10.99±1.29	0.00±0.00	0.25±0.43	5.09±0.43	7.99±1.59	57.52±0.81	0.00±0.00	18.15±0.40	0.44	53.74±17.36	0.14±0.05	10.27±1.52
alkali-treated	7.31±0.37	2.18±1.66	0.00±0.00	1.25±1.09	31.62±5.70	55.10±4.42	0.00±0.00	2.54±0.92	12.43	22.02±6.85	0.62±0.07	101.7±17.76
spark oxidized	12.71±1.58	0.36±0.22	0.71±0.63	0.75±0.67	3.29±0.36	65.70±1.196	10.93±0.22	5.55±0.85	0.59	27.33±3.56	0.85±0.02	171.06±41.79

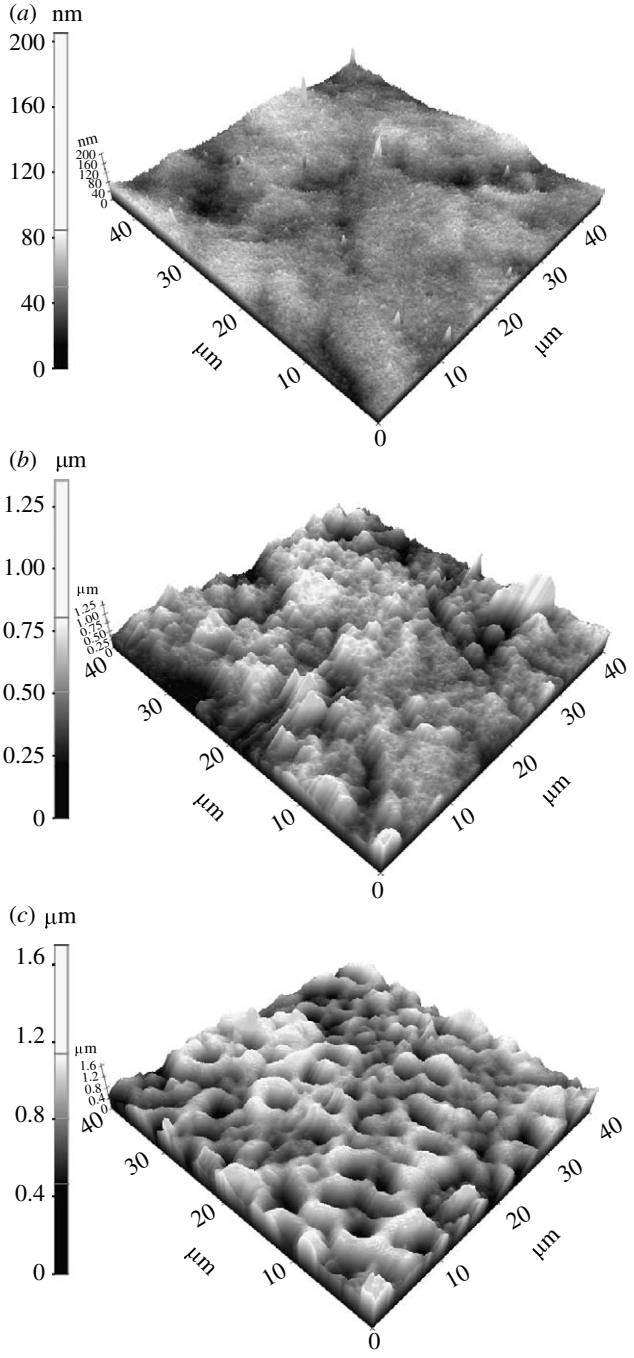

Figure 1. AFM images of (*a*) ground, (*b*) alkali-treated and (*c*) spark oxidized nitinol samples.

3.2. Surface chemical composition measurements

The chemical composition of the sample surfaces is compiled in table 1. Carbon contamination as measured by XPS was in the moderate/low level (7.3–12.1%) for all the samples. XPS examination without etching the surface was carried out to assess the chemical composition of the top few nanometres (1–5 nm) of the outermost layer. This layer of alkali-treated samples was very rich in nickel that was predominantly in the oxide state as indicated from the binding energy (E_b=854.8 eV; figure 2*a*). A significant increase of nickel in the outer layer of alkali-treated samples

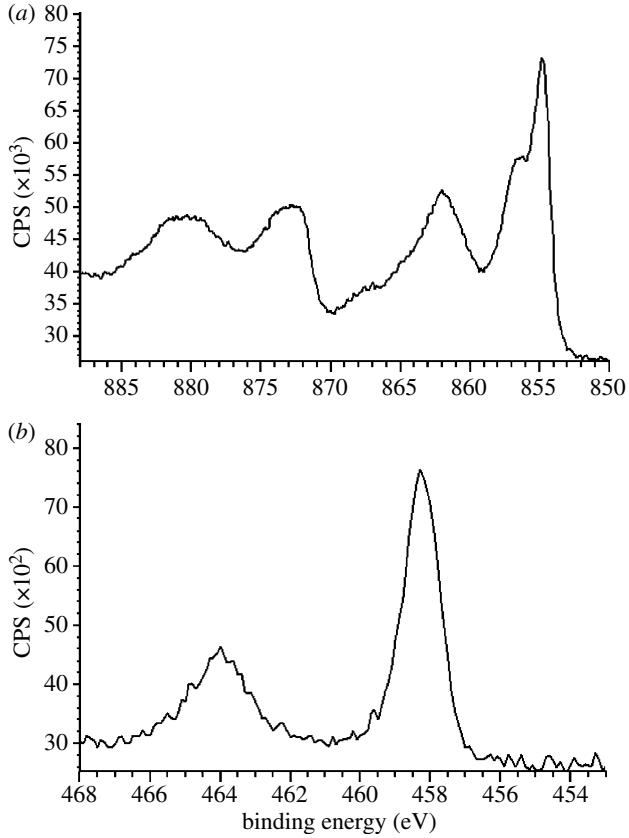

Figure 2. XPS detailed spectra of surface-treated nickel–titanium. (*a*) Ni2p for alkali-treated samples and (*b*) Ti2p for spark oxidized samples.

caused an increase in the Ni/Ti ratio. This ratio was the highest for these samples ($(Ni/Ti)^{BNT}=12.43$) compared with ground ($(Ni/Ti)^{NT}=0.44$) and spark oxidized ($(Ni/Ti)^{SP}=0.59$) samples. The alkali-treated samples also contained approximately 2 at% calcium and 3 at% sodium. On the other hand, the spark oxidized samples had the lowest content of nickel and titanium. For the spark oxidized sample, nickel as well as titanium (TiO_2, $E_b=458$ eV) was also present in oxide forms (figure 2*b*). Moreover, the samples contained approximately 10% phosphorus that corresponded with phosphorus oxide ($E_b=134.2$ eV). Ground samples, however, were composed of titanium, nickel, oxygen, sodium and carbon. Titanium had two main peaks; the first peak was recognized at $E_b=454.1$ eV, which corresponded to metallic titanium (Ti), and the second peak at $E_b=458.5$ eV, which corresponded to TiO_2. The presence of metallic form of titanium suggested the thickness of the oxide layer to be in the range 2–4 nm. Oxygen was recognized as O_2 ($E_b=531.1$ eV), hydroxide, Ni_2O_3 ($E_b=531.5$ eV), H_2O and double-bonded carbon–oxygen (–C=O; $E_b=532.8$ eV). Nickel for these samples was recognized mainly in metallic form ($E_b=852.2$ eV) with a small amount of nickel oxides (NiO and Ni_2O_3). Unexpectedly on the ground samples, some sodium was also found ($E_b=1071.7$ eV), which corresponded with the metallic form and also combined with titanium oxide ($NaTiO_6$).

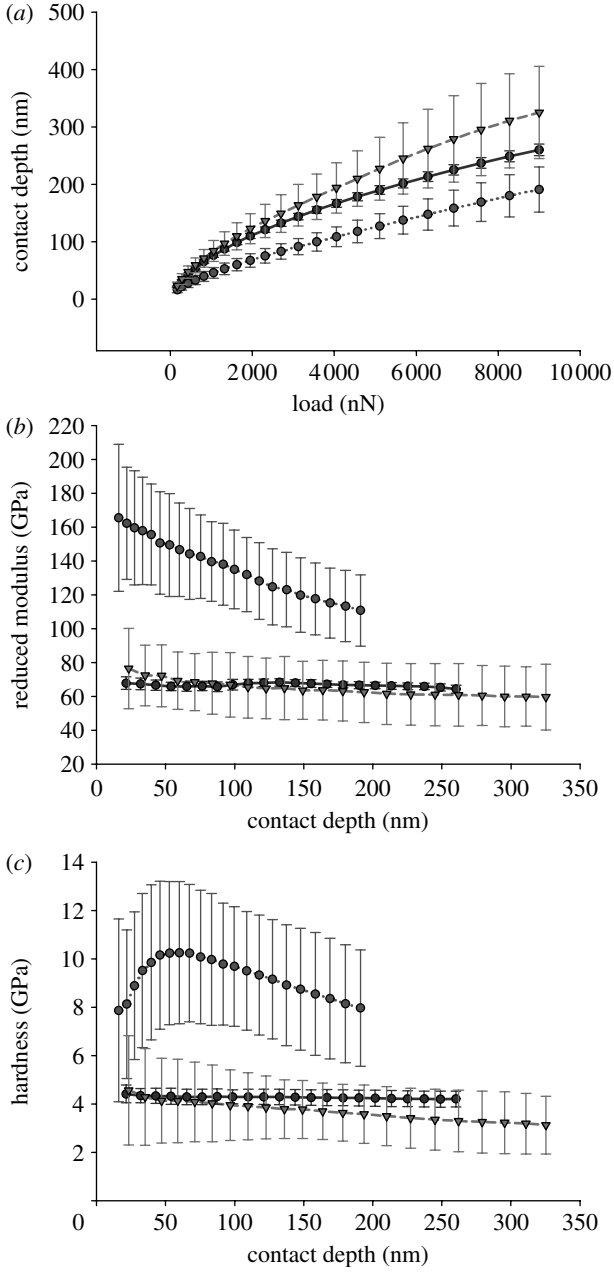

Figure 3. Results of nanoindentation tests. (*a*) Contact depth versus applied load, (*b*) reduced modulus versus contact depth and (*c*) hardness versus contact depth for three types of samples NT (dark shaded circles), BNT (light shaded circles) and SP (shaded triangles).

3.3. CA measurements

CA measurement revealed differences in wettability of the samples after treatment as given in table 1. The CA value dropped to 22° and 27° for alkali and oxidized samples, respectively, compared with 53° for the ground samples.

3.4. Nanohardness tests

Results of nanoindentation tests are shown in figure 3*a–c*. Initial minimum applied load (168.89 μN) resulted in different contact depth for all three groups of samples. The starting contact depth for ground sample was 21.46 nm, which is greater than the estimated thickness

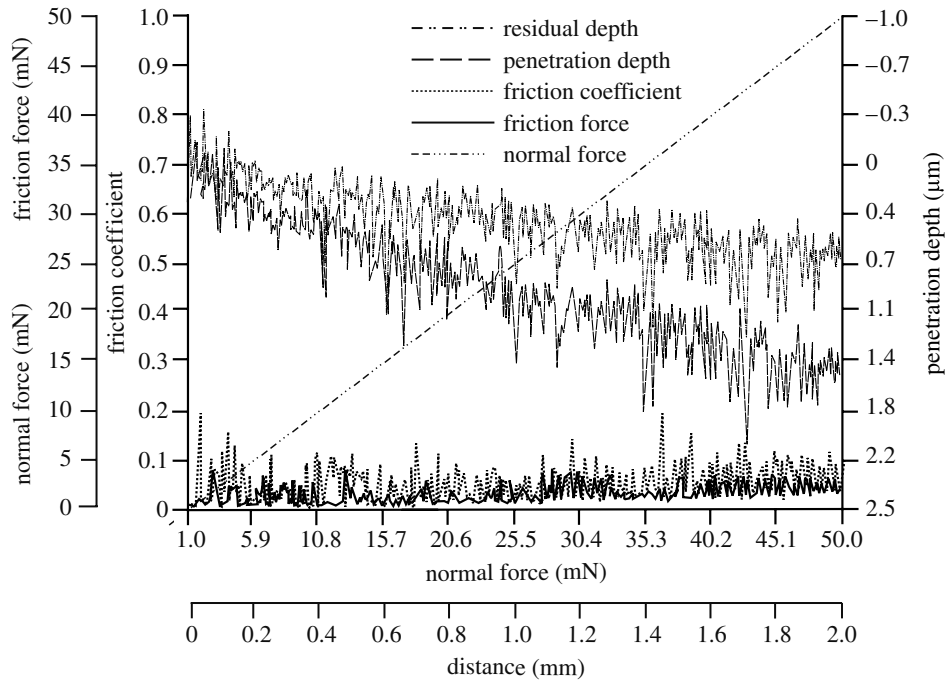

Figure 4. Friction force (mN), friction coefficient and penetration depth (μm) of the spark oxidized nitinol sample as obtained from the scratch test.

Table 2. Specific start, peak and finish temperatures for austenite→martensite and martensite→austenite transformation as obtained from DSC measurements during heating and cooling of the samples.

	heating			cooling		
sample	A_s (°C)	peak (°C)	A_f (°C)	M_s (°C)	peak (°C)	M_f (°C)
ground	5.55±2.74	18.28±0.94	27.74±1.39	14.06±0.62	4.64±0.61	−5.09±0.80
600	12.09±1.18	30.79±1.37	42.30±1.32	−9.19±1.87	−14.64±0.74	−19.66±0.31

of the oxide layer; therefore, these results represent the properties of the substrate. Initial contact depth for BNT and SP samples was 15.99 and 23.27 nm, respectively. An increase in the applied load resulted in differences in the growth of the depth for each of the studied samples. The highest increase in the contact depth was observed for spark oxidized samples, while the lowest was for alkali-treated samples (figure 3*a*).

Analysis of the reduced modulus showed that the highest values were observed for alkali-treated samples; initial $E_r = 165.49$ GPa, and the modulus values were decreasing with increasing depth of the penetration. For the ground sample, the modulus was reduced (64.85 GPa for the lowest applied force), and only minor fluctuations of its value was observed with increasing depth of penetration. On the other hand, the moduli of the spark oxidized samples were comparable with those of the ground samples with no significant differences, and the initial value was 76.46 GPa, which dropped to 59.63 GPa for 9000 μN (figure 3*b*).

Regarding the hardness values, the greatest value was observed for alkali-treated samples. Hardness for the lowest applied force was 7.87 GPa and increased with increase in the contact depth (load) reaching a maximum 10.26 GPa for 60 nm depth (load 1623.01 μN). Further increase in the load caused a decrease in the hardness (figure 3*c*). For the spark oxidized and ground samples, however, the initial values were 4.57 and 4.42 GPa. Increasing applied load caused steady, slow decrease in hardness for spark oxidized samples, while no changes were observed for ground samples.

3.5. Nanoscratch and nanotribo tests

Nanoscratch tests were carried out for alkali-treated and spark oxidized nitinol samples. Critical load (CL) for spark oxidized samples was 39.4 mN and the indenter calculated maximal Hertzian pressure was 26 GPa (table 2). For the alkali-treated samples, CL was 9.3 mN and maximal Hertzian pressure was 47 GPa. The maximum penetration depth was 1.7 and 1.1 μm for the spark oxidized and alkali-treated samples, respectively (figures 4 and 5). Residual depth measurements for both samples showed a similar trend with approximately 0.25 μm higher depth for spark oxidized samples. The difference between the penetration and residual depth was 0.1 μm greater for spark oxidized samples. For oxidized samples, delamination of the layer occurred only at certain points along the scratch (figure 6*a*) after exceeding a critical force. No scratch was observed on the surface before breakage of the layer, which occurred for significantly greater force and further distance compared with

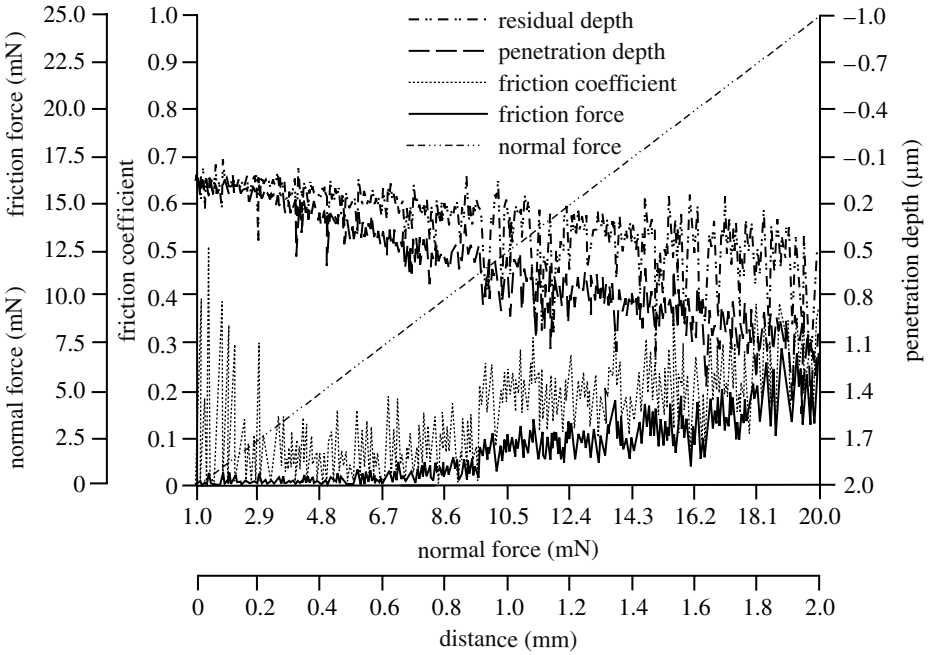

Figure 5. Friction force (mN), friction coefficient and penetration depth (μm) of the alkali-treated nitinol sample as obtained from the scratch test.

alkali-treated samples. Delamination of the outer layer for alkali-treated samples occurred later than critical force was recorded (break of the layer). These results suggested that the top layer of sodium hydroxide-treated (alkali-treated) samples was more brittle than the oxidized samples. By considering the friction coefficients and friction force, the results showed that these parameters were twice as low for spark oxidized samples (maximum 0.1 and 2.5 mN; figures 3 and 4), and they steadily increased along the test duration. For the alkali-treated samples in the middle of the test, the values increased. This increase could suggest a change in the properties with thickness or perhaps it is an actual measurement of the underlying substrate. The final suggestion can be further supported by analysis of the obtained images (figure 6), where it can be seen that the indenter reached the substrate.

Nanotribo tests showed that for ground samples, the initial friction is high for approximately 80 s (figure 7); then the stylus broke through the very thin natural oxide layer and reached the substrate (figure 8*a*). The plot from 80 s onwards represents the friction of the substrate. For alkali-treated samples, the mean value of coefficient of friction was 0.69 (figure 7), and it steadily increased along the test. The spark oxidized samples showed a large and steady increase in friction with wear. Because the ball did not reach the substrate (figure 8*c*), this increase was observed and a larger value of the coefficient was detected. The friction of the spark oxidized samples increases more than compared with alkali-treated samples. The results also demonstrated that the ground samples wear gradually with time, and the substrate was reached after 80 s. Alkali treatment, however, improved the wear resistance, but the top layer was also removed gradually. The spark oxidized samples had the highest wear resistance (figures 7 and 8). A steady increase in friction and observation of the surface after the tests demonstrated good wear resistance of the oxide layer obtained via spark oxidation, in the nanowear tests.

3.6. Transformation temperature measurements

DSC analysis showed that heat treatment altered the peak temperature of the transformation since the untreated ground samples had a transformation temperature of 18.25 ± 0.88°C, while thermally treated samples had a significantly higher ($p < 0.05$) transformation temperature compared with the untreated samples (30.82 ± 1.38°C) during heating cycle (figure 9). Start and finish temperatures of the transformation austenite → martensite (during heating) and martensite → austenite (during cooling) were also altered by the heat treatment (table 2). Transformation from austenite to martensite during heating started at a higher temperature for the heat-treated samples (figure 9). Reverse transformation (during cooling), however, started at a lower temperature.

3.7. X-ray diffraction

Recorded XRD spectra revealed a difference in the structure of the nickel–titanium after heat treatment at 600°C. The structure of the ground samples was austenitic: one dominating peak at $2\theta = 42.9°$, which corresponds with austenite phase (110) (figure 10). After heat treatment, apart from the austenite peak at $2\theta = 42.9°$, additional peaks at angles 41.1°, 43.5° and 44.5° were present and they corresponded with the martensite phase (−111), (020) and (012) (figure 10).

3.8. Corrosion tests

The results of corrosion tests are compiled in table 3 and figure 11. The average corrosion potentials for the ground

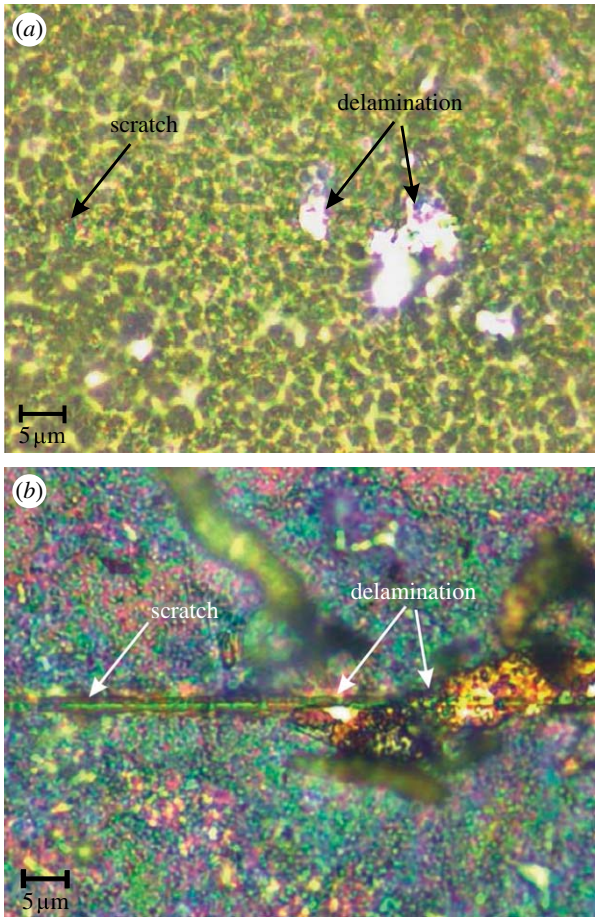

Figure 6. LM images of the scratches on the surfaces after scratch tests for (*a*) spark oxidized and (*b*) alkali-treated samples.

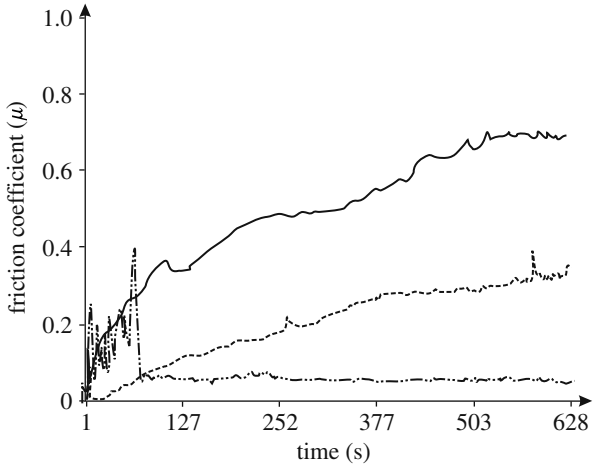

Figure 7. Friction coefficient as a function of time for alkali-treated and spark oxidized compared with the polished nitinol samples as obtained from the nanotribo test. Solid line, spark oxidized; dashed line, alkali-treated; dash-dotted line, ground.

samples were −207 mV. Similar values were observed for alkali-treated samples (average −205 mV). The highest corrosion potential, however, was observed for spark oxidized samples (average −20 mV). In the next step, polarization curves were recorded and transpassivation potential, polarization resistance and corrosion

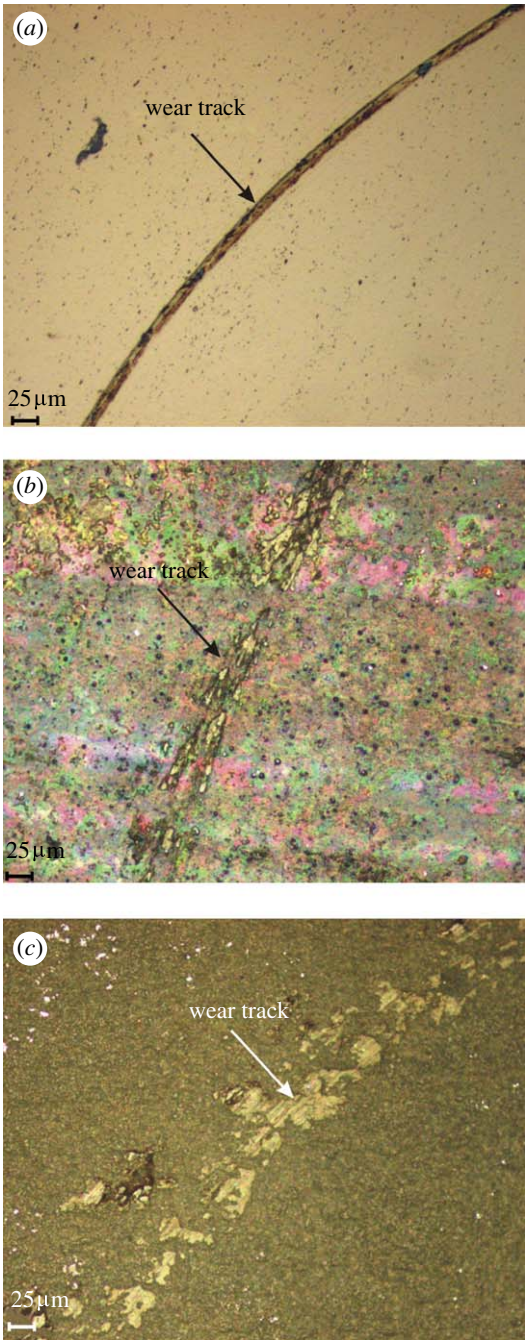

Figure 8. Images of the surfaces after nanotribo test. (*a*) Polished surface, (*b*) alkali-treated and (*c*) spark oxidized nitinol samples.

current density were evaluated. The lowest value of transpassivation potential was observed for ground samples (1105 mV), while the highest was recorded for alkali-treated samples (1422 mV). The average potential for the spark oxidized samples was 1364 mV.

Recorded reverse polarization curves revealed significant differences between the samples (figure 11). For both ground and spark oxidized samples and when polarization direction was diverted, i.e. the current reached 1 mA cm^{-2}, a rapid drop of the current was observed—repassivation with no pitting corrosion observed. An increase in the current was related to the oxygen evolution. However, for alkali-treated samples after reaching a current of 1 mA cm^{-2} and diverting

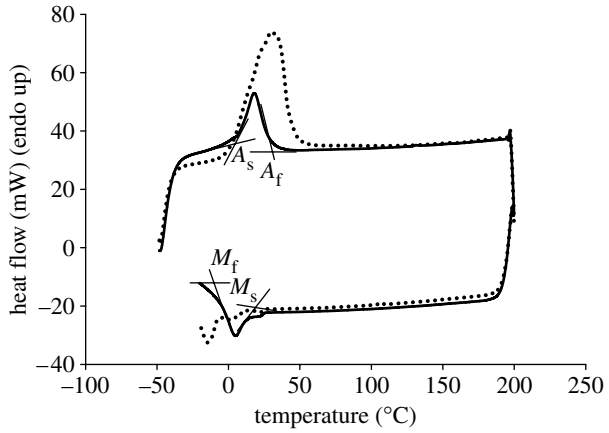

Figure 9. Transformation temperature for nickel–titanium before (solid line, ground) and after annealing at 600°C (dotted line).

Table 3. Results of corrosion potential, polarization resistance, transpassivation potential and corrosion current for ground, alkali-treated and spark oxidized samples.

sample	E_{cor} (mV)	R_p (kΩ cm^2)	E_B (mV)	i_{cor} (nA cm^{-2})
NT	−207±29	368±84	1105±199	10.61±3.10
BNT	−205±43	312±102	1422±72	23.16±8.24
SP	−20±6	437±72	1364±102	24.23±9.32

polarization direction, a significant increase in current density was observed and a large number of pits appeared on the surface. The recorded potential corresponded to breakdown potential, and a large surface area under the reverse curve was also observed (figure 11). Repassivation for alkali-treated samples occurred at potentials that were close to the corrosion potential. Analysis of the polarization resistance showed that there were no significant differences between the samples. Nevertheless, corrosion current density was the lowest for ground samples (10.6 nA cm^{-2}), while for both SP and BNT it was at a similar level of approximately 24 nA cm^{-2}.

3.9. Results of thickness measurements of oxide layer

Measurements of the thickness of the layer on the obtained cross-section images revealed that the greatest thickness was observed for spark oxidized samples Pa1 = 3.154 µm (figure 12*a*). Thickness of the layer was uniform on the whole area of the samples. Additionally, it was observed that the structure of this layer is porous. For alkali-treated samples the thickness varied in different areas of the sample and was in the range 0.7–1.196 µm (figure 12*b*). For the reference ground sample SEM/FIB analysis did not enable one to evaluate the thickness of the layer. Despite the fact of using very high magnification the layer was not identified on the substrate (figure 12*c*). The thickness was below the resolution of the instrument. It is assumed on the basis of previous XPS analysis that

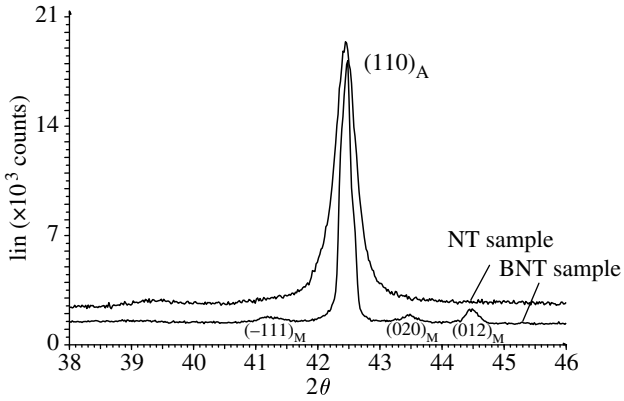

Figure 10. XRD spectra for ground and alkali-treated samples.

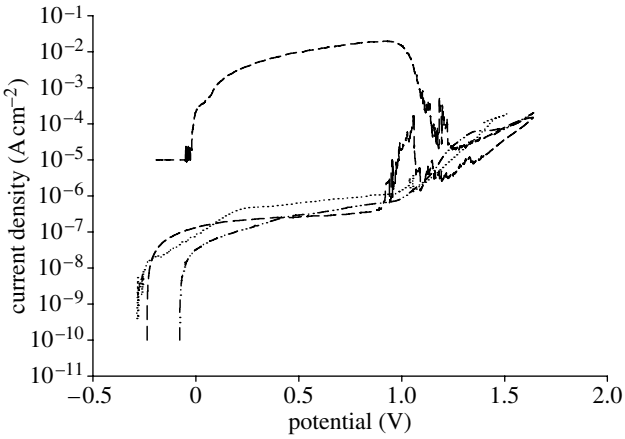

Figure 11. Anodic polarization curves recorded in HBSS at 36°C for ground, alkali-treated and spark oxidized samples. Dotted line, NT; dash-dotted line, SP; dashed line, BNT.

the natural oxide layer present on the ground samples is very thin, and its thickness did not exceed 4 nm.

4. DISCUSSION

In the literature, a lot of space is devoted to the issue of surface preparation of implants and its influence on biological (cell and microbial) response. Biological aspects are crucial and also the surface plays the most important role in contact with tissue. The most important factors that are underlined in biomedical implant evaluation are chemical composition of the surface and its topography (Green *et al.* 1997; Wen *et al.* 1998; Filip *et al.* 2001; Chen *et al.* 2003, 2004; Cui *et al.* 2005; Garcia *et al.* 2006; Sul *et al.* 2006; Kawakita *et al.* 2007; Byon *et al.* 2007). However, consideration about dental, maxillofacial and orthopaedic implants should include aspects connected with implant insertion, bearing forces and frictional interaction between the implant and the surrounding musculoskeletal tissue. All these matters lead to surface changes that can impair the biological properties of the implant, and these changes take place when the surface layer is scratched, removed or cracked due to wear. This implies that investigations of both mechanical and

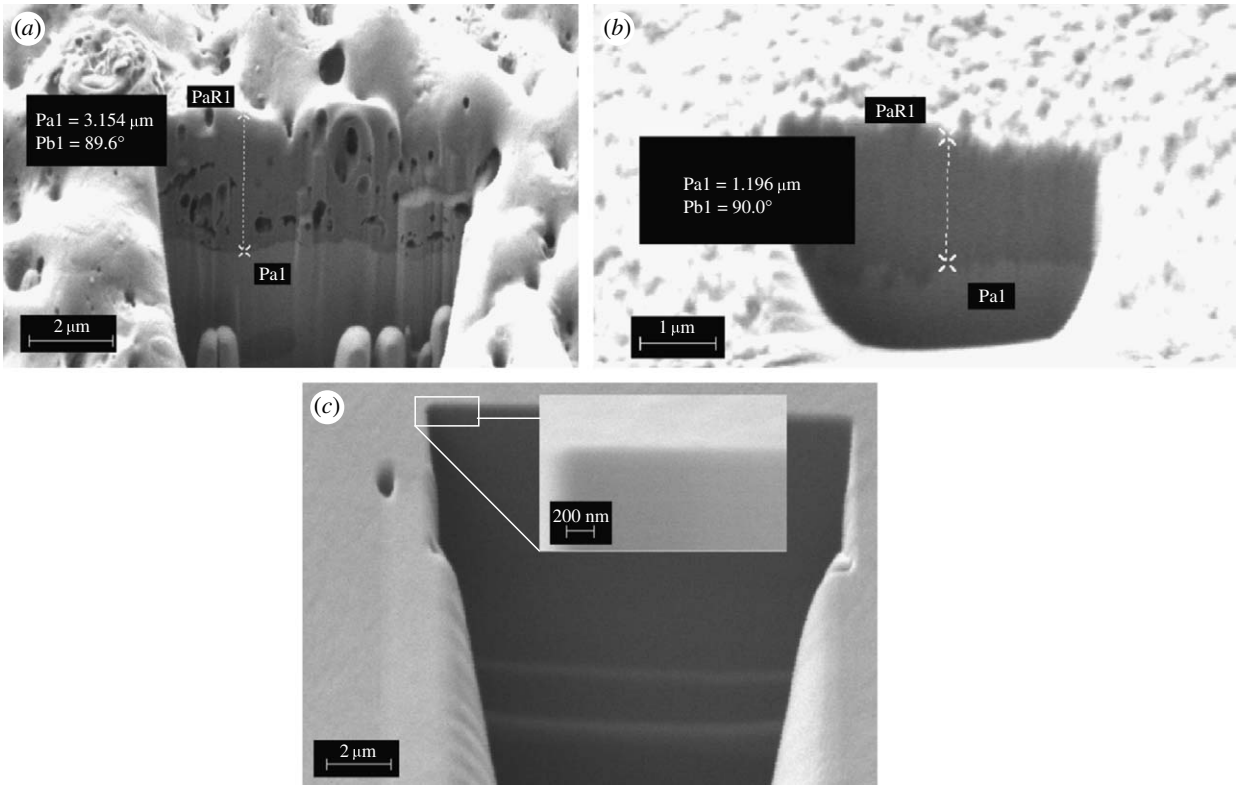

Figure 12. Cross section of the layer on the samples. (*a*) Spark oxidized, (*b*) alkali-treated and (*c*) ground nickel–titanium.

tribological properties of the surface must be carried out for these implants in addition to biological aspect research. Here in this study, the authors made an attempt to investigate from a wear and mechanical point of view the suitability of two types of surface treatments for nickel–titanium alloy. These treatments were previously used for titanium and its alloys to improve corrosion, wear and also biological properties of the alloys for biomedical applications (Wen *et al.* 1998; Wang *et al.* 2000; Hassel 2004; Rocher *et al.* 2004; Chrzanowski *et al.* 2005; Kokubo 2005; Mändl *et al.* 2006; Shukla & Balasubramaniam 2006).

In this study, nitinol samples were prepared in two different ways: alkali followed by thermal treatment and spark oxidation; the samples treated in both ways were compared with a ground sample that was used as a reference. Before any surface treatments, all the studied samples were ground under the same conditions as the reference samples to eliminate the effect of mechanical grinding as it has been reported that the mechanical grinding introduces stress and deformation to the outer layer of Ni–Ti, which can lead to local structural changes (Hassel 2004). Alkali treatment in NaOH was chosen due to the reported positive results of this treatment on titanium and its alloys (Wang *et al.* 2000; Kokubo 2005; Wei *et al.* 2007). This treatment increased the surface energy and resulted in incorporation of sodium ions onto the surface. As a result of the treatment a sodium titanate layer was created and then due to exchange of Na^+ ions with H_3O^+ during immersing in SBF, Ti–OH was created, which in turn enhances formation of an apatite layer (Kokubo 2005). Spark oxidation using direct current gave a rough structure with a characteristic pinhole appearance (Chrzanowski 2006; Byon *et al.* 2007). Additionally, this rough layer contained large amounts of phosphorous ions. This kind of roughness and chemical composition combination is believed to trigger positive cell response (Kokubo *et al.* 1996; Armitage & Chrzanowski 2007; Byon *et al.* 2007; Kawakita *et al* 2007). However, it was presented by Kawakita *et al.* (2007) that the structure and chemical composition of the oxide layer on nickel–titanium alloy is dependent on anodization conditions. They also demonstrated that oxidation using high-voltage pulse wave form current resulted in an amorphous oxide layer that contained very low nickel content and an improvement in corrosion resistance.

Despite the fact that oxidation parameters play an important role in the properties of the oxide layer, variances in this process were not considered in this study and the conditions of oxidation were chosen according to previous authors' experience using high-voltage oxidation with direct current (Chrzanowski *et al.* 2005). This was also presented to have a positive influence on corrosion resistance of titanium alloys (Ti6Al4V, Ti6Al7Nb).

Roughness measurements and topography observations showed that both treatments increased the R_a value. Compared with the ground samples, the roughness increased to 0.62 and 0.85 μm for alkali treated and spark oxidized, respectively. The spark oxidized surface is regularly pitted and porous as evidenced from SEM/FIB images of the layer cross section. Thickness of the layer was approximately 3.1 μm and was uniform on the sample. Topography of the alkali-treated samples was less regular with some scratches that appeared during the surface treatment in NaOH. The treatment resulted in different thickness of the layer on

the samples, which was in the range 0.7–1.2 μm. Increase in the surface roughness and irregularities in topography is recognized as a positive, as it may have an impact on cell response (Ronold *et al.* 2003). CA measurements revealed that both treatments significantly increased wettability of the surface. The drop of the CA was 5° lower for spark oxidized samples. The obtained increase in roughness together with the decrease in the CA suggested that these two types of treatment could possibly improve bioactivity of the surface (Kujala *et al.* 2003; Kokubo 2005; Yi *et al.* 2006; Yousefpour *et al.* 2007).

The chemical composition measurements revealed that the alkali treatment increased the concentration of nickel in the outer layer. XPS measurements without sputtering enable the evaluation of the chemical composition of a layer approximately 2–5 nm in thickness. This thin film on the alkali-treated samples was enriched with nickel that was present in the oxide form (figure 2*a*). The Ni/Ti ratio was very high (12.43), and is of major concern due to high risk of side effects related to nickel release. This undesirable effect of a surge of nickel content on the outer part of the layer can be a decisive factor on the suitability of this kind of treatment for medical application. As is well known, the nickel oxide layer is not stable under physiological conditions and can be dissolved causing an increase in local nickel concentration in tissues (Ryhänen 1999). In addition, alkali treatment enriched the surface with sodium and calcium (table 1). This calcium could be derived from the reagents used to prepare the NaOH solution and also from the ceramic crucibles used for heat treatment of the samples. Unlike the alkali treatment, the nickel concentration was the lowest for the spark oxidized samples; the surface of these samples was composed mainly of titanium dioxide, nickel (Ni_2O_3) and phosphorus oxides.

On the surface of ground samples, some sodium was detected; this sodium could be from the water used to clean samples as evidenced by the ICP measurement, which revealed that the water used for cleaning and rinsing the samples contained approximately 125 ppb of sodium. This could explain the source of sodium in these samples.

Nanomechanical evaluation of the surface properties, including nanoindentation, nanoscratch and nanotribo tests, provides information concerning the surface mechanical properties, wear resistance and adhesion. Nanoindentation tests showed differences in hardness after surface treatments. The hardness value obtained for the ground samples represented those of the underlying substrate rather than the surface layer as the minimum recorded contact depth was approximately 22 nm, which suggested that the layer should be approximately 200 nm. On the other hand, XPS analysis showed that this oxide layer is no greater than 4 nm, due to the fact that metallic nickel and titanium were observed, which in turn meant that we had signal from the substrate and thickness can be approximated to be no greater than 4 nm. The greatest hardness was observed for alkali-treated samples. The hardness increased with depth of the indentation reaching a maximum of 10.26 GPa for 60 nm contact depth (5% of total thickness of the layer; figure 3*c*). The highest hardness of the alkali-treated samples could be related to different crystallographic structure of these samples revealed in XRD analysis. The XRD results showed the presence of martensite phase in the heat-treated samples (figure 10), which caused an increase in hardness. It was also demonstrated from DSC data that at room temperature the heat-treated samples were partly transformed, and may contain both phases (austenite and martensite), which further support the findings from XRD (figures 9 and 10). Ground samples, however, had only austenitic structure at room temperature. This finding suggested that thermal treatment influenced hardness and material properties during the nanomechanical tests, which were done at room temperature as it was assumed that structures of the ground and thermally treated samples during the tests were different as for heat-treated samples the material was partly transformed. The results suggest that heat treatment caused the appearance of martensite phase at room temperature.

The hardness of the spark oxidized samples was at a similar level as recorded for the ground sample, while it was significantly lower than that of the alkali-treated samples. Despite the porous structure of the layer of spark oxidized samples (figure 12*a*), nanoindentation test showed that the nanohardness was uniform on the cross section of the layer, whose thickness was 3.1 μm.

The reduced modulus obtained from nanoindentation tests was the greatest for alkali-treated samples. No significant differences were observed between spark oxidized and ground samples. Nevertheless, some differences in the penetration depth were detected. The highest penetration depth was obtained for spark oxidized and the lowest for alkali treated (figure 3), which is in agreement with hardness tests.

Results of the scratch test for ground samples, which had a natural thin oxide film (approx. 2–4 nm, estimated on the basis of XPS measurements), might represent the substrate not the actual oxide layer wear properties, and in such case it would not give any additional information about adhesion of the film to the surface. Owing to the instrument force feedback loop control, the force applied on the samples was not affected by the surface topography. Moreover, the prescan procedure allows measurement of the real penetration depth during the scratch, and characterizes the elastic recovery using the post-scan procedure.

Scratch tests also confirmed the previous findings; penetration depth was greater for spark oxidized samples due to the lower hardness and greater thickness. Scratch tests showed that adhesion of the top layer was good for spark oxidized samples. Hertzian pressure was 26 GPa. These tests were carried out with different indenter radii to minimize the influence of the underlying substrate and the differences in the thickness of the surface layer. Additionally, observation of the scratches showed that the alkali-treated surface is more brittle. For alkali-treated samples, greater hardness and Hertzian pressure (47 GPa) was observed. For the alkali-treated samples, the indenter gradually penetrated the layer causing delamination after

exceeding the critical force. Likewise for spark oxidized samples, delamination occurred also after exceeding the critical force (figure 6), after significantly longer distance but lower Hertzian pressure. This demonstrated better adhesion of the top layer on alkali-treated samples compared with spark oxidized samples. However, different test parameters that were used resulting in different fields of pressure in the coating, in the substrate and at the interface do not allow for direct comparison of both coatings.

Analysis of the residual depth data showed that alkali-treated samples had 0.2 μm greater difference between penetration depth and residual depth. This could suggest higher plastic recovery. The results also showed that better frictional properties were obtained for the spark oxidized samples as demonstrated by the frictional force from the scratch tests; this force was twice as low for the spark oxidized compared with the alkali-treated samples. Further analysis of the nanowear properties showed that both treatments increased wear resistance compared with ground samples, and the alkali treatment doubled the coefficient of friction. A gradual increase in the friction coefficient was observed for alkali-treated samples, which may suggest a progressive wear of the top layer and a change in the properties with depth (figure 7). The rise of the friction could be attributed to the associated wear of the top oxide layer, and hence the ball starts to wear the substrate (figure 8*b*). However, due to much higher roughness and thinner oxide layer, the final value came from the mixture of friction of the ball against the oxides and the substrate. For the spark oxidized samples the ball did not reach the substrate (this is the friction of the steel ball; figure 8*c*), which could be attributed to the higher roughness detected for the spark oxidized samples and greater thickness. Observations of the friction coefficient for spark oxidation samples showed a steady increase in the friction, which suggests that substrate was not reached; thus it showed wear resistance properties compared with the other samples.

Corrosion tests revealed that pitting corrosion occurred only on alkali-treated samples. However, these samples had greater transpassivation potential (in this case it was also the breakdown potential; figure 11). The annealing process at 600°C after immersing in sodium hydroxide is assumed to have an influence on corrosion resistance due to the fact that nickel tarnishes and is pyrophoric when heated in air (Vandenkerckhove *et al.* 2004; Greenwood & Earnshaw 2007). Appearance of the ferromagnetic martensite phase could also have an influence on lowering the corrosion resistance. As is well known, the two-phase (martensite and austenite) materials are more prone to corrosion compared with single-phase austenitic materials (Perez 2004). In addition, creation of nickel and titanium complexes with sodium and calcium, which in turn make the structure heterogeneous could also be implicated in the reduction of the corrosion resistance. This type of structure is more prone to corrosion than the uniform oxide layer, which was present on spark oxidized samples. The lowest corrosion current density, which was analysed at $E_{(i=0)}$ (Tafel's method), was observed for ground samples, and it was approximately two times lower than that for the other analysed samples.

Unlike alkali-treated samples, both ground and spark oxidized samples did not show pitting corrosion, and the change in the polarization direction caused repassivation of the surface. The highest corrosion potential was observed for spark oxidized samples, which could be due to the chemical composition of the top layer that was composed mainly of corrosion resistant titanium dioxide.

In spite of the fact that the alkali treatment resulted in good adhesion of the surface layer to the underlying substrate and enhanced its wear resistance, the chemical composition of this layer and its tendency towards pitting corrosion disqualify this treatment for being used for medical applications. From the wear resistance point of view, the spark oxidized samples showed relatively good properties compared with the ground samples, and they also showed an improvement in the corrosion resistance.

5. SUMMARY

Under the experimental conditions presented in this study, the following conclusions can be drawn.

(i) Alkali treatment increased the surface roughness, surface energy and hardness. It also improved wear resistance compared with ground samples. Adhesion of the 1.2 μm thick layer to the substrate was very good. However, this treatment decreased the corrosion resistance and caused a significant increase in nickel content, which make this kind of treatment not suitable for biomedical applications.

(ii) Spark oxidation resulted in the formation of a relatively thick 3.1 μm rough, porous and pitted oxide layer that has high wear resistance and good adhesion to the underlying substrate. It also improved the wear resistance compared with alkali-treated and reference (ground) samples. Moreover, it enhanced the corrosion resistance—greater corrosion and transpassivation potential and lower current density in the passive area.

(iii) Thermal treatment at 600°C increased the transformation temperature of the nitinol and caused the appearance of martensite phase in the structure.

This work was supported by EU FP6, IEF Marie Curie Action, CSM and Hysitron. Also funding from EPSRC is gratefully acknowledged.

REFERENCES

Armitage, D. A. & Chrzanowski, W. 2007 Surface preparation of Ni–Ti alloy using alkali, thermal treatments and spark oxidation. *Proc. Eur. Soc. Biomater., SFM106, Brighton, UK.*

Byon, E., Jeong, Y., Takeuchi, A., Kamitakahara, M. & Ohtsuki, C. 2007 Apatite-forming ability of micro-arc

plasma oxidized layer of titanium in simulated body fluids. *Surf. Coat. Technol.* **201**, 5651–5654. (doi:10.1016/j.surfcoat.2006.07.051)

Cheng, Y. & Zheng, Y. F. 2006*a* Deposition of TiN coatings on shape memory NiTi alloy by plasma immersion ion implantation and deposition. *Thin Solid Films* **515**, 1358–1363. (doi:10.1016/j.tsf.2006.03.041)

Cheng, Y. & Zheng, Y. F. 2006*b* Surface characterization and electrochemical studies of biomedical NiTi alloy coated with TiN by PIIID. *Mater. Sci. Eng. A* **438-440**, 1146–1149. (doi:10.1016/j.msea.2005.12.073)

Chen, M. F., Yang, X. J., Liu, Y., Zhu, S. L., Cui, Z. D. & Man, H. C. 2003 Study on the formation of an apatite layer on NiTi shape memory alloy using a chemical treatment method. *Surf. Coat. Technol.* **173**, 229–234. (doi:10.1016/S0257-8972(03)00733-3)

Chen, M. F., Yang, X. J., Hu, R. X., Cui, Z. D. & Man, H. C. 2004 Bioactive NiTi shape memory alloy used as bone bonding implants. *Mater. Sci. Eng. C* **24**, 497–502. (doi:10.1016/j.msec.2003.11.001)

Chrzanowski, W. 2006 Corrosion behavior of Ti6Al7Nb alloy after different surface treatments. *J. Achiev. Mater. Manuf. Eng.* **18**, 67–71.

Chrzanowski, W., Szewczenko, J., Tyrlik-Held, J., Marciniak, J. & Zak, J. 2005 Influence of the anodic oxidation on the physicochemical properties of the Ti6Al4V ELI alloy. *J. Mater. Process. Technol.* **162–163**, 163–168. (doi:10.1016/j.jmatprotec.2005.02.203)

Chu, C. L., Chung, C. Y., Lin, P. H. & Wang, S. D. 2005 Fabrication and properties of porous NiTi shape memory alloys for heavy load-bearing medical applications. *J. Mater. Process. Technol.* **169**, 103–107. (doi:10.1016/j.jmatprotec.2005.03.002)

Cui, F. Z., Chung, C. Y., Zhou, J., Pu, Y. P. & Lin, P. H. 2005 Fabrication and characteristics of bioactive sodium titanate/titania graded film on NiTi shape memory alloy. *J. Biomed. Mater. Res. A* **75**, 595–602. (doi:10.1002/jbm.a.30465)

Filip, P., Lausma, J., Musielak, J. & Mazanec, K. 2001 Structure and surface of TiNi human implants. *Biomaterials* **22**, 2131–2138. (doi:10.1016/S0142-9612(00)00404-X)

Firstov, G. S., Vitchev, R. G., Kumar, H., Blanpain, B. & Van Humbeeck, J. 2002 Surface oxidation of NiTi shape memory alloy. *Biomaterials* **23**, 4863–4871. (doi:10.1016/S0142-9612(02)00244-2)

Garcia, C., Cere, S. & Duran, A. 2006 Bioactive coatings deposited on titanium alloys. *J. Non-Cryst. Solids* **352**, 3488–3495. (doi:10.1016/j.jnoncrysol.2006.02.110)

Green, S. M., Grant, D. M. & Wood, J. V. 1997 XPS characterisation of surface modified Ni–Ti shape memory alloy. *Mater. Sci. Eng. A* **224**, 21–26. (doi:10.1016/S0921-5093(96)10563-3)

Greenwood, N. N. & Earnshaw, A. 2007 *Chemistry of the elements*. Norwich, NY: Knovel.

Grosgogeat, B., Jablonska, E., Vernet, J. M., Jaffrezic, N., Lissac, M. & Ponsonnet, L. 2006 Tribological response of sterilized and un-sterilized orthodontic wires. *Mater. Sci. Eng. C* **26**, 267–272. (doi:10.1016/j.msec.2005.10.050)

Gu, Y. W., Tay, B. Y., Lim, C. S. & Yong, M. S. 2005 Characterization of bioactive surface oxidation layer on NiTi alloy. *Appl. Surf. Sci.* **252**, 2038–2049. (doi:10.1016/j.apsusc.2005.03.207)

Hassel, A. W. 2004 Surface treatment of NiTi for medical applications. *Minim. Invasiv. Ther. Allied Technol.* **13**, 240–247. (doi:10.1080/13645700410020278)

Ju, X. & Dong, H. 2006 Plasma surface modification of NiTi shape memory alloy. *Surf. Coat. Technol.* **201**, 1542–1547. (doi:10.1016/j.surfcoat.2006.02.022)

Kawakita, J., Stratmann, M. & Hassel, A. W. 2007 High voltage pulse anodization of a NiTi shape memory alloy. *J. Electrochem. Soc.* **154**, C294–C298. (doi:10.1149/1.2720768)

Kobayashi, S., Ohgoe, Y., Ozeki, K., Sato, K., Sumiya, T., Hirakuri, K. K. & Aoki, H. 2005 Diamond-like carbon coatings on orthodontic archwires. *Diam. Relat. Mater.* **14**, 1094–1097. (doi:10.1016/j.diamond.2004.11.036)

Kokubo, T. 1998 Apatite formation on surfaces of ceramics, metals and polymers in body environment. *Acta Mater.* **46**, 2519–2527. (doi:10.1016/S1359-6454(98)80036-0)

Kokubo, T. 2005 Design of bioactive bone substitutes based on biomineralization process. *Mater. Sci. Eng. C* **25**, 97–104. (doi:10.1016/j.msec.2005.01.002)

Kokubo, T., Miyaji, F. & Kim, H. M. 1996 Spontaneous formation of bonelike apatite layer on chemically treated titanium metals. *J. Am. Ceram. Soc.* **79**, 1127–1129. (doi:10.1111/j.1151-2916.1996.tb08561.x)

Kujala, S., Ryhänen, J., Danilov, A. & Tuukkanen, J. 2003 Effect of porosity on the osteointegration and bone ingrowth of a weight-bearing nickel–titanium bone graft substitute. *Biomaterials* **24**, 4691–4697. (doi:10.1016/S0142-9612(03)00359-4)

Liu, X. *et al.* 2007 Structure and wear properties of NiTi modified by nitrogen plasma immersion ion implantation. *Mater. Sci. Eng.* **444**, 192–197. (doi:10.1016/j.msea.2006.08.071)

Man, H. C., Ho, K. L. & Cui, Z. D. 2006 Laser surface alloying of NiTi shape memory alloy with Mo for hardness improvement and reduction of Ni^{2+} ion release. *Surf. Coat. Technol.* **200**, 4612–4618. (doi:10.1016/j.surfcoat.2005.04.034)

Mändl, S., Fleischer, A., Manova, D. & Rauschenbach, B. 2006 Wear behaviour of NiTi shape memory alloy after oxygen-PIII treatment. *Surf. Coat. Technol.* **200**, 6225–6229. (doi:10.1016/j.surfcoat.2005.11.070)

Marciniak, J., Chrzanowski, W., Paszenda, Z., Szade, J. & Wniarski, W. 2007*a* Carbon layers on the Ti6Al7Nb implants surface. *Biomater. Eng.* **46**, 12–15.

Marciniak, J., Chrzanowski, W., Zak, J. & Rajchel, B. 2007*b* Structure modification of surface layers of Ti6Al4V ELI implants. *Key Eng. Mater.* **254–256**, 387–390.

Ni, W., Cheng, Y. T. & Grummon, D. S. 2006 Wear resistant self-healing tribological surfaces by using hard coatings on NiTi shape memory alloys. *Surf. Coat. Technol.* **201**, 1053–1057. (doi:10.1016/j.surfcoat.2006.01.067)

Parashos, P. & Messer, H. H. 2005 Uptake of rotary NiTi technology within Australia. *Aust. Dent. J.* **50**, 251–257.

Perez, N. 2004 *Eelectrochemistry and corrosion science*. Boston, MA: Kluwer Academic Publishers.

Rocher, P., El Medawar, L., Hornez, J.-C., Traisnel, M., Breme, J. & Hildebrand, H. F. 2004 Biocorrosion and cytocompatibility assessment of NiTi shape memory alloys. *Scr. Mater.* **50**, 255–260. (doi:10.1016/j.scriptamat.2003.09.028)

Ronold, H. J., Lyngstadaas, S. P. & Ellingsen, J. E. 2003 Analysing the optimal value for titanium implant roughness in bone attachment using a tensile test. *Biomaterials* **24**, 4559–4564. (doi:10.1016/S0142-9612(03)00256-4)

Ryhänen, J. 1999 *Biocompatibility evaluation of nickel–titanium shape memory alloy*. Oulu, Finland: OulunYliopisto.

Shevchenko, N., Pham, M.-T. & Maitz, M. F. 2004 Studies of surface modified NiTi alloy. *Appl. Surf. Sci.* **235**, 126–131. (doi:10.1016/j.apsusc.2004.05.273)

Shukla, A. K. & Balasubramaniam, R. 2006 Effect of surface treatment on electrochemical behavior of CP Ti,

Ti–6Al–4V and Ti–13Nb–13Zr alloys in simulated human body fluid. *Corros. Sci.* **48**, 1696–1720. (doi:10.1016/j.corsci.2005.06.003)

Sul, Y. T., Jeong, Y., Johansson, C. & Albrektsson, T. 2006 Oxidized, bioactive implants are rapidly and strongly integrated in bone. Part 1—experimental implants. *Clin. Oral Implan. Res.* **17**, 521–526. (doi:10.1111/j.1600-0501.2005.01230.x)

Vandenkerckhove, R., Chandrasekaran, M., Vermaut, P., Portier, R. & Delaey, L. 2004 Corrosion behaviour of a superelastic Ni–Ti alloy. *Mater. Sci. Eng. A* **378**, 532–536. (doi:10.1016/j.msea.2003.11.072)

Wang, X. X., Hayakawa, S., Tsuru, K. & Osaka, A. 2000 A comparative study of *in vitro* apatite deposition on heat-H_2O_2-, and NaOH-treated titanium surfaces. *J. Biomed. Mater. Res.* **52**, 172–178. (doi:10.1002/1097-4636(200010)52:1<171::AID-JBM22>3.0.CO;2-O)

Wei, D. Q., Zhou, Y., Jia, D. C. & Wang, Y. M. 2007 Characteristic and *in vitro* bioactivity of a microarc-oxidized TiO_2-based coating after chemical treatment. *Acta Biomater.* **3**, 817–827. (doi:10.1016/j.actbio.2007.03.001)

Wen, H. B., de Wijn, J. R., Cui, F. Z. & de Groot, K. 1998 Preparation of bioactive Ti6Al4V surfaces by a simple method. *Biomaterials* **19**, 215–221. (doi:10.1016/S0142-9612(97)00232-9)

Wen, C. E., Xu, W., Hu, W. Y. & Hodgson, P. D. 2007 Hydroxyapatite/titania sol–gel coatings on titanium–zirconium alloy for biomedical applications. *Acta Biomater.* **3**, 403–410. (doi:10.1016/j.actbio.2006.10.004)

Yan, W. 2006 Theoretical investigation of wear-resistance mechanism of superelastic shape memory alloy NiTi. *Mater. Sci. Eng. A* **427**, 348–355. (doi:10.1016/j.msea.2006.05.005)

Yang, H., Qian, L. M., Zhou, Z. R., Ju, X. H. & Dong, H. S. 2007 Effect of surface treatment by ceramic conversion on the fretting behavior of NiTi shape memory alloy. *Tribol. Lett.* **25**, 215–224. (doi:10.1007/s11249-006-9169-6)

Yi, J. H., Bernard, C., Variola, F., Zalzal, S. F., Wuest, J. D., Rosei, F. & Nanci, A. 2006 Characterization of a bioactive nanotextured surface created by controlled chemical oxidation of titanium. *Surf. Sci.* **600**, 4613–4621. (doi:10.1016/j.susc.2006.07.053)

Yousefpour, M., Afshar, A., Chen, J. & Zhang, X. 2007 Bioactive layer formation on alkaline-acid treated titanium in simulated body fluid. *Mater. Des.* **28**, 2154–2159. (doi:10.1016/j.matdes.2006.06.005)

Zheng, Y. F. & Huang, B. M. 2001 *Superelastic and thermally activated TiNi alloys and their applications in dentistry.* Uetikon-Zurich, Switzerland: Trans Tech Publications Ltd.